

Uncertainty Quantification in Detecting Choroidal Metastases on MRI via Evolutionary Strategies

Bala McRae-Posani¹, Andrei Holodny¹, Hrithwik Shalu^{2*}, Joseph N Stember^{1*}

¹Memorial Sloan Kettering Cancer Center, Department of Radiology
1275 York Avenue, New York, NY 10065
mskcc.org

²Indian Institute of Technology Madras, Department of Aerospace Engineering
IIT P.O., Chennai, Tamil Nadu, India, 600036
iitm.ac.in

Abstract

Uncertainty quantification plays a vital role in facilitating the practical implementation of AI in radiology by addressing growing concerns around trustworthiness. Given the challenges associated with acquiring large, annotated datasets in this field, there is a need for methods that enable uncertainty quantification in small data AI approaches tailored to radiology images. In this study, we focused on uncertainty quantification within the context of the small data evolutionary strategies-based technique of deep neuroevolution (DNE). Specifically, we employed DNE to train a simple Convolutional Neural Network (CNN) with MRI images of the eyes for binary classification. The goal was to distinguish between normal eyes and those with metastatic tumors called choroidal metastases. The training set comprised 18 images with choroidal metastases and 18 without tumors, while the testing set contained a tumor-to-normal ratio of 15:15.

We trained CNN model weights via DNE for approximately 40,000 episodes, ultimately reaching a convergence of 100% accuracy on the training set. We saved all models that achieved maximal training set accuracy. Then, by applying these models to the testing set, we established an ensemble method for uncertainty quantification. The saved set of models produced distributions for each testing set image between the two classes of normal and tumor-containing. The relative frequencies permitted uncertainty quantification of model predictions. Intriguingly, we found that subjective features appreciated by human radiologists explained images for which uncertainty was high, highlighting the significance of uncertainty quantification in AI-driven radiological analyses.

Introduction

Radiology artificial intelligence (AI) requires Uncertainty quantification (UQ)

It is widely appreciated that for artificial intelligence (AI) to gain traction in real-life clinical deployment, single-point predictions must be contextualized by uncertainty quantification (UQ). UQ can help ensure that AI predictions are trustworthy and reliable, helping to overcome clinician hesitation about using them in practice (Faghani et al. 2023, 2022; McCrindle et al. 2021). By incorporating UQ, AI

researchers can produce responsible AI better positioned to benefit patients directly. Although not phrased in those terms, the importance of UQ for patient management is reflected in the fact that several radiology report lexicons have been designed expressly to convey the certainty or uncertainty of diagnoses (Panicek and Hricak 2016; Kendall and Gal 2017).

UQ must work in settings of sparse data

Despite UQ's key role in responsible AI, there has hitherto been no practical way to evaluate uncertainty for small data scenarios. Practical radiology AI requires being able to learn in the small data regime since obtaining and labeling images is time-consuming and tedious and excludes rare conditions or presentations.

Hence, the radiology AI research community needs small data UQ. In this work, we will demonstrate a way to quantify uncertainty for classifying small sets of radiological images.

We quantified uncertainty using a small data training approach based on evolutionary strategies

In particular, we will show that UQ with small training sets is feasible when we use a small data training approach called Deep Neuroevolution (DNE) (Stember and Shalu 2022; Stember, Young, and Shalu 2023; Purkayastha et al. 2022). We have chosen to use DNE because it has been shown to achieve high training and testing set accuracies for small numbers of brain MRIs, and can generalize to heterogeneous data.

We studied eye MRI exams to demonstrate how researchers can embed UQ into DNE's small-data AI approach. In particular, we performed binary classification between normal eyes and those with metastatic lesions, called choroidal metastases. This provides a nice illustration of computing and studying UQ when only limited data are present.

Methodology

From recent literature, it has been established that Evolutionary Strategies (ES)-based parametric optimization of Neural Networks are scalable alternatives in the regime of Data-Efficient Deep Learning (Stember, Young, and Shalu

*These authors contributed equally.

2023; Such et al. 2017). In this work we employ an ES based optimization strategy called Deep Neuroevolution (DNE) to form Deep ensembles. DNE has the valuable property of permitting the semiautomated acquisition of an ensemble of different, but all valid, models. We can quantify epistemic uncertainty in unseen testing set data using the model ensembles. A straightforward advantage for gradient-free optimization methods compared to autograd(Ketkar et al. 2021)-/gradient descent-based methods is the flexibility granted on the constraint/objective function used. For autograde-based deep learning, the objective function is the loss of the output with respect to a known human-annotated label or target value. For our purposes, we form a scalar reward (fitness) based on the sum of True Positives and True Negatives that acts as our evaluation metric.

A brief discussion of Evolutionary Strategies (ES)

The form of ES used throughout this study can be simplified into three major components. To perform parametric optimization of a deep neural network, firstly, a population of models with size $2p$ is formed from a reference model by asynchronous perturbations of the model weights. Suppose the weights of the reference model at some iteration standpoint t is w_t , then p pairs of perturbed models are formed as the positive/negative perturbations of the model weights. More formally, the weights of a pair of perturbed models ($\pm p_i$) are obtained by perturbing the reference model weights (at iteration t) with a random vector (ϵ_i) as shown in Equation 1, where μ is the magnitude factor of the perturbations:

$$w_{p_i}^{\pm} = w_t \pm \mu \epsilon_i. \quad (1)$$

Note that the values of perturbation vector ϵ_i for all our purposes are randomly sampled from a standard normal distribution. Secondly, we evaluate the perturbed models with a given training set (\mathcal{D}_T), and the metric formed (R_i^{\pm}) is normalized as per the scheme shown in Equation 2.

$${}^N R_i^{\pm} = \frac{\max(0, \log_2(p+1) - \log_2(R_i^{\pm} + 1))}{\sum_{i=0}^{2p-1} \max(0, \log_2(p+1) - \log_2(R_i^{\pm} + 1))} + \frac{1}{2p} \quad (2)$$

Finally, we update the reference model with gradients computed per the SPSA (Spall 1992) scheme. More formally the gradient estimates formed by evaluating on p pairs of perturbed models with their respective performance metrics (${}^N R_i^{\pm}$) is as shown in Equation 3.

$$\nabla_{w_t} \mathcal{R} = \frac{1}{p} \sum_{i=1}^p \frac{{}^N \mathcal{R}_i^+(w_t + \mu \epsilon_i) - {}^N \mathcal{R}_i^-(w_t - \mu \epsilon_i)}{2\mu} \quad (3)$$

A noteworthy advantage of the optimization scheme is the asynchronous nature of the gradient updates and their scalable nature in terms of the population size p . That is, relative exploration of the parameter space could be improved with a large enough population size (Assunção et al. 2019), enabling greater diversity regarding neuron pathways in the formed models.

Estimating prediction uncertainty using deep ensembles

In this section, we outline the method used for quantifying the epistemic uncertainty of models trained using the ES-based optimization scheme. We base our method on the fact that there is diversity in the population of models formed at each iteration, including after training has reached convergence. DNE’s convergence properties enable a semi-automated and reliable ensemble-based UQ scheme. DNE has been shown to converge monotonically to high training and testing set accuracies (Stember and Shalu 2022; Stember, Young, and Shalu 2023; Stember et al. 2023; Purkayastha et al. 2022) DNE converges monotonically toward high training and testing set accuracies. Hence, after convergence, all models both:

- Valid because they are highly accurate. and
- Unique, because of the random perturbations applied to network weights at each step of DNE.

This permits a straightforward, semiautomated, and reliable method for UQ:

1. Train the CNN with DNE until convergence has been reached.
2. Once some minimum number N_{conv} of training steps/generations have transpired since convergence, training can be terminated.
3. Simply collect the last N_{conv} model weights. N_{conv} represents the post-convergence training iterations, and represents the desired number of ensemble members for UQ. In general, higher N_{conv} is preferred due to better statistical sampling. An advantage of DNE-based UQ is that we can readily collect as many models as desired to obtain sufficient statistical sampling for UQ, since all we need to do is wait for convergence and then collect/save models.
4. Once we have our ensemble of models $\{\mathcal{F}_i\}_{i=1}^{N_{conv}}$, we can compute a distribution of class predictions C for each testing set image I : $\{C_i\}_{i=1}^{N_{conv}} = \{\mathcal{F}_i(I)\}_{i=1}^{N_{conv}}$. Of note, here we have a binary classifier, so C can be either metastatic tumor (\mathcal{T}) or normal/tumor-free (\mathcal{N}).
5. Quantify the uncertainty by first computing its inverse, the Shannon entropy, S . For the two classes, tumor (\mathcal{T}) and normal (\mathcal{N}), this becomes: $S = (\mathcal{T} \cdot \log_2(\mathcal{T}) + \mathcal{N} \cdot \log_2(\mathcal{N}))$.

Algorithm 1 more formally defines the process by which models of unique neural schemes are saved during the optimization process. Note that a baseline criteria for model selection with respect to the training set performance is used as the minimum requirement. Additionally the **is unique** criteria in *line 14* of Algorithm 1 is set such that temporally unique models would be saved. This enables us to scale the ensemble constituents beyond the sparse set of unique validation performance values. For unseen data, the ensemble of the saved models obtained using Algorithm 1 is used to estimate the predictive distribution. The same is used to estimate epistemic uncertainty of the predicted label.

Algorithm 1: Uncertainty Quantification using multi-model ensemble: An evolutionary strategies based approach.

Input: Dataset(s) : $\mathcal{D}_T = \{I_i, l_i\}, \mathcal{D}_V = \{I_i, l_i\}$
Parameters: $\{\alpha, p, N_{epochs}, R_{max}^{\mathcal{D}_T}\}$
Output: Set of trained Neural Networks : $\{\mathcal{N}_i\}$

```

1: Let  $t = 0$ .
2:  $\mathcal{M}_S[w_t]$  : Randomly Initialized Reference Model.
3: while  $t \leq N_{epochs}$  do
4:   Perturb and Evaluate
5:   for  $i$  ranging  $[1, p]$  do
6:     Using Equation 1
7:     Form pair of perturbed models :  $\mathcal{M}[w_{p_i}^{\pm}]$ 
8:     Obtain performance metrics
9:     Evaluate  $\mathcal{M}[w_{p_i}^{\pm}]$  on  $\mathcal{D}_T$  and  $\mathcal{D}_V$ 
10:    Store evaluations :  $R_i^{\pm}$  and  ${}_V R_i^{\pm}$ 
11:   end for
12:   Store models for deep ensemble
13:   if  $(R_i^{\pm} == R_{max}^{\mathcal{D}_T})$  and  $({}_V R_i^{\pm}$  is unique) then
14:     Save Model :  $\mathcal{M}[w_{p_i}^{\pm}]$ 
15:   end if
16:   Update Reference Model
17:   Using Equation 2
18:   Compute normalized metrics :  ${}^N R_i^{\pm}$ 
19:   Using Equation 3
20:   Compute gradient update for reference model
21:    $w_{t+1} = w_t - \alpha \times \nabla_{w_t} \mathcal{R}$ 
22: end while
23: return Saved Models

```

Experimental Setup

We evaluate the algorithm in a limited data setting where the class of images has inherently low data availability to emphasize the method’s necessity. Namely, we employ the method for the detection of choroidal metastases from radiological image slices obtained through Magnetic Resonance Imaging (MRI) of the brain. We used T2-weighted images because they provide adequate contrast between the hyper-intense aqueous humor and the lower intense metastatic lesions.

We aimed to assess the performance of our method relative to the widely used Dropout-based uncertainty quantification (UQ) technique employing autograd (Gal and Ghahramani 2016; Lakshminarayanan, Pritzel, and Blundell 2017). Accordingly, we computed uncertainties using both methods. The results of the Deep NeuroEvolution (DNE)-based UQ are presented herein, while the details of the Dropout-based UQ performance can be found in Appendix A.

Data Acquisition and Availability

This was an IRB-approved study. The data used in this study was acquired while maintaining the highest privacy standards possible and accounting for all ethical considerations.

We retrospectively obtained MRI brain images from patients with radiology report texts describing choroidal metastases for our tumor-containing cases. We also obtained

normal MRI brains for our normal cases. For the tumor-containing cases, we chose T2-weighted images. We selected the axial slice that best exemplified the lesions. Additionally, we manually cropped every image to focus on the right and left globes specifically. The custom dataset used for this study is available from the corresponding author upon reasonable request.

Outline of Experiments

We evaluated DNE’s ability to learn from training data, generalize to a separate testing set, and quantify uncertainty under two distinct neural network settings. First, we tried a single-branched architecture (Figure 6) where only a candidate image slice serves as input. The motivation for doing so was to help the network prioritize inter-class pattern recognition. Second, we employed a two-input (branched) architecture (Figure 1) to facilitate symmetric pattern recognition between left and right globes. Figures 6 and 1 illustrate these convolutional neural network (CNN) architectures. All model parameters were fixed after basic hyperparameter tuning via grid-search (Bergstra and Bengio 2012). A detailed set of hyperparameters used are included in the respective figure captions.

Data distribution

We base our experiments on the class-balanced dataset (1:1). We performed two-fold cross-validation:

1. The first fold featured 18 training set image pairs (images of the bilateral orbits) and 15 testing image pairs.
2. In the second fold, the training and testing data were flipped, for a 15:18 ratio.

These ratios were chosen to challenge our approach more than is traditionally done in deep learning. Doing so emphasizes DNE’s ability to learn and generalize from very small training datasets.

Results

Primary evaluations are done so as to evaluate the performance of the proposed setting in terms of relative generalizability; the-best performing model acquired a testing set accuracy of 93.33 ± 3.33 upon model cross-validation.

UQ class	Tumor	Normal
Correct with low uncertainty	9 (27.3%)	13 (39.4%)
High uncertainty	17 (51.2%)	19 (57.8%)
Incorrect with low uncertainty	7 (21.2%)	1 (3.0%)

Table 1: Distribution of UQ classes. For purposes of evaluation high uncertainty is formally defined here as Shannon entropy greater than 0.2.

Next, we acquired predictive distributions of the deep ensemble of models as produced by Algorithm 1. Considering relative entropy as a measure, a subdivision was formed between the predictive distributions so as to form three distinct

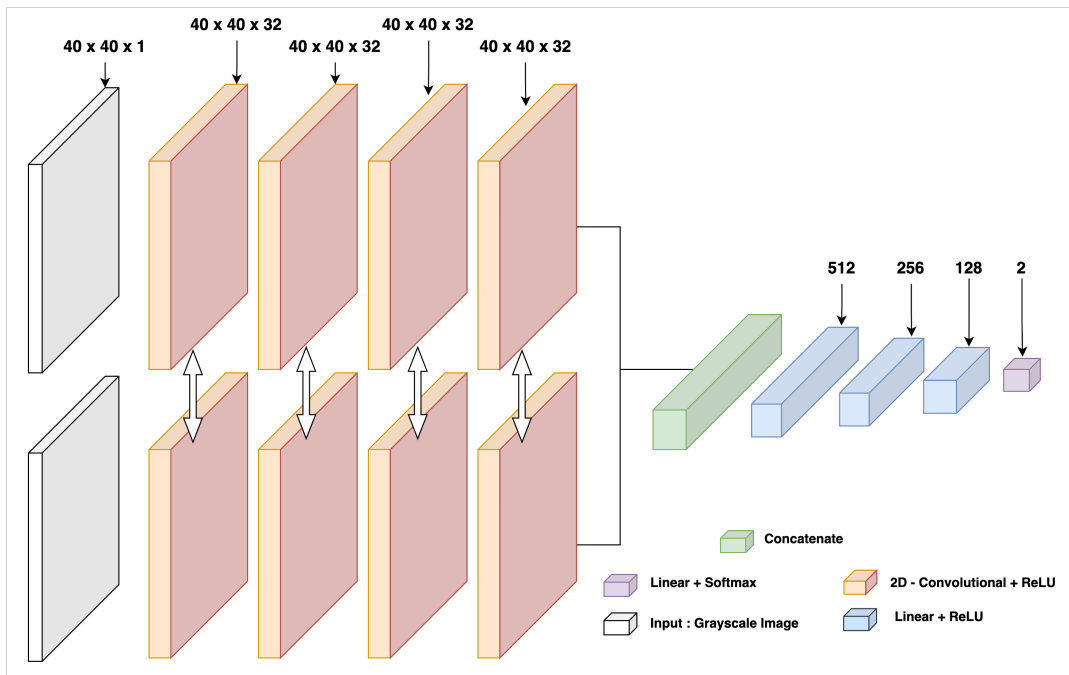


Figure 1: Multi-input convolutional neural network architecture used for the binary classification (tumor vs normal) of choroidal metastases from Brain MRI slices. The network takes as input two grayscale images, each of size (40, 40, 1) : (Height, Width, Channel), and produces a Softmax distribution over the respective classes of interest. Note that the bidirectional arrows represent shared weights between blocks. Respective convolutional channels (for CNN layers) and Neuron counts (Linear layers) are marked against each block. Respective hyperparameters used in training the network as per Algorithm 1 : $\{\alpha = 0.12, p = 40, N_{epochs} = 10^5, R_{max}^{D_T} = 30 \text{ or } 36\}$

classes of uncertainties estimated. For the best-performing model out of the two architectures the same is outlined in Table 1. Figure 2 shows the averaged convergence trends shown under evaluations. Further analysis and results on supportive studies are added in Appendix sections A-B. Training and testing code for all models and settings were developed using the Pytorch (Paszke et al. 2019) framework in python. All experiments were conducted on a virtual interface (Bisong and Bisong 2019) using an 8 core 9th gen intel i7 processor and a Tesla P4 GPU.

Discussion

Reliable artificial intelligence is of prime importance to medical image analysis because the predictions are high stakes, and trustworthiness is paramount. As such, our models must be able to quantify predictive uncertainty. Quantifying uncertainty has been of interest to many recent studies associated with radiological image analysis (Qendro et al. 2021; Abdar et al. 2021; Selvan et al. 2020).

Our work expands prior research via the introduction of small data AI techniques and the examination of their relative strengths with respect to quantifying epistemic uncertainty for out-of-distribution data (Yang and Fevens 2021; Lambert et al. 2022). Although the performance factors of ES-based methods (Stember and Shalu 2022; Ahmadian et al. 2021; Zhou and Feng 2018) on small datasets are impressive and well investigated, this work builds upon the

same to provide a means for a seemingly valid uncertainty estimation. Note that a distinguishing factor of our method that sets it apart from prior literature is the guarantee of solution validity for each component of the deep ensemble formed. In other words, on comparison with Monte-Carlo dropout or other forms of deep ensemble formations in an effort to quantify predictive uncertainty, the explicit constraint (as imposed in Algorithm 1) on the permissible training set accuracy/performance required for each component of the ensemble allows us to form a more valid form of uncertainty modeling.

From the results outlined in Table 1, it is clear that the out-of-distribution data in the testing set largely constitutes the sub-class of relatively high uncertainty and could be identified as possible points of miss-classification. However, it's worth noting that the relative insights that such data points could provide in augmenting the training set are valuable. That's when considering a continual learning model, that requires periodic augmentation of its training set so as to improve generalizability, the proposed setting could be used as straightforward mechanism for relative selection of data-points from unseen data. It is worth mentioning that the vast majority of UQ studies are focused on estimating epistemic uncertainty (Abdar et al. 2022; Cifci 2023), which reflects model uncertainty related to not having seen the needed size and range of data during training to generalize enough to perform on unseen data. Other forms of uncertainty, such

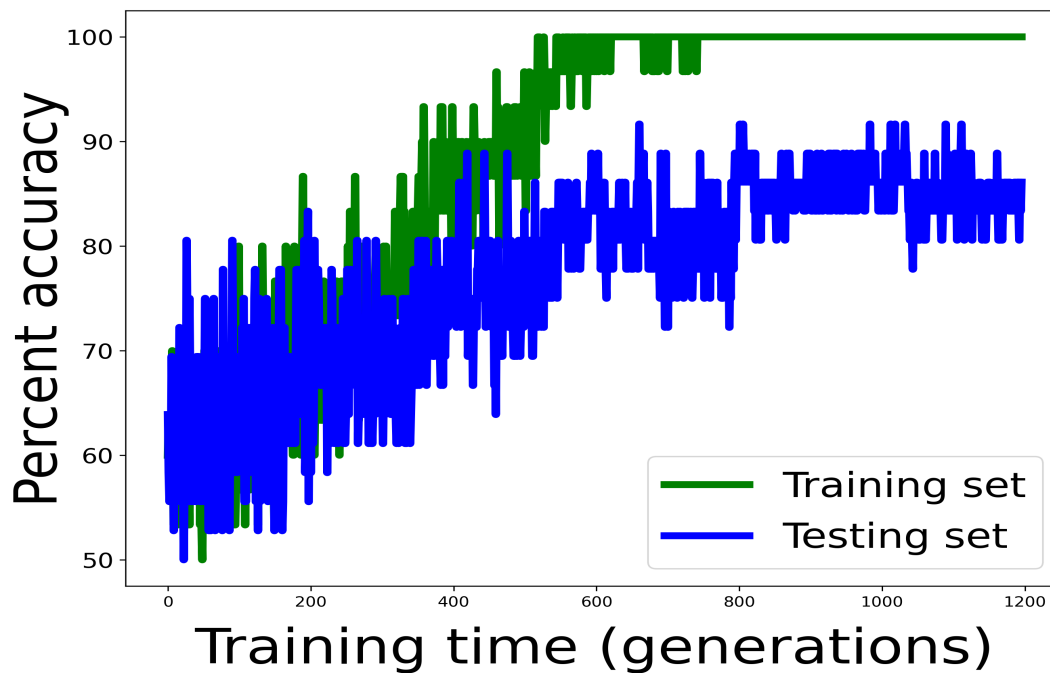


Figure 2: Accuracy versus training time in generations during training of the CNN from Figure 1. This is an average formed from 5 repeated runs of one of the 2-fold cross-validation training runs, with a training set size of 15 and testing set size of 18.

as Aleatoric uncertainty, which relates to inherent randomness, are less explored. Note that a practical extension of the method outlined could be to form a set of model communities emerging from different sets of labeling sources (such as institutions or experts) in an effort to quantify other prominent forms of uncertainties. However, in this proof of concept, such depths were not explored.

Limitations

As previously mentioned in the discussions, there are cases where uncertainty quantification methods could miss out completely while estimating epistemic uncertainty for unseen data. Figures 3 and 4 illustrate the core limitations that come about due to the limitations in the visible feature space of the images or the inherent noise features which could potentially show up in the practical implementation of the method outlined in this study. Another major limitation of the method is the space complexity required to store the distinct models to form the deep ensembles. In future work, we hope to address the above-mentioned shortcomings with better-optimized model configurations (Alibrahim and Ludwig 2021) or by relatively simplifying the space complexity using model quantization or quantization aware training (Stewart et al. 2021; Ferianc et al. 2021).

References

Abdar, M.; Fahami, M. A.; Rundo, L.; Radeva, P.; Frangi, A. F.; Acharya, U. R.; Khosravi, A.; Lam, H.-K.; Jung, A.; and Nahavandi, S. 2022. Hercules: Deep hierarchical attentive multilevel fusion model with uncertainty quantification

for medical image classification. *IEEE Transactions on Industrial Informatics*, 19(1): 274–285.

Abdar, M.; Pourpanah, F.; Hussain, S.; Rezazadegan, D.; Liu, L.; Ghavamzadeh, M.; Fieguth, P.; Cao, X.; Khosravi, A.; Acharya, U. R.; et al. 2021. A review of uncertainty quantification in deep learning: Techniques, applications and challenges. *Information fusion*, 76: 243–297.

Ahmadian, S.; Jalali, S. M. J.; Islam, S. M. S.; Khosravi, A.; Fazli, E.; and Nahavandi, S. 2021. A novel deep neuroevolution-based image classification method to diagnose coronavirus disease (COVID-19). *Computers in biology and medicine*, 139: 104994.

Alibrahim, H.; and Ludwig, S. A. 2021. Hyperparameter optimization: Comparing genetic algorithm against grid search and bayesian optimization. In *2021 IEEE Congress on Evolutionary Computation (CEC)*, 1551–1559. IEEE.

Assunção, F.; Lourenço, N.; Machado, P.; and Ribeiro, B. 2019. Fast denser: Efficient deep neuroevolution. In *European conference on genetic programming*, 197–212. Springer.

Bergstra, J.; and Bengio, Y. 2012. Random search for hyperparameter optimization. *Journal of machine learning research*, 13(2).

Bisong, E.; and Bisong, E. 2019. Google colabatory. *Building machine learning and deep learning models on google cloud platform: a comprehensive guide for beginners*, 59–64.

Cifci, M. A. 2023. A Deep Learning-Based Framework for Uncertainty Quantification in Medical Imaging Using the

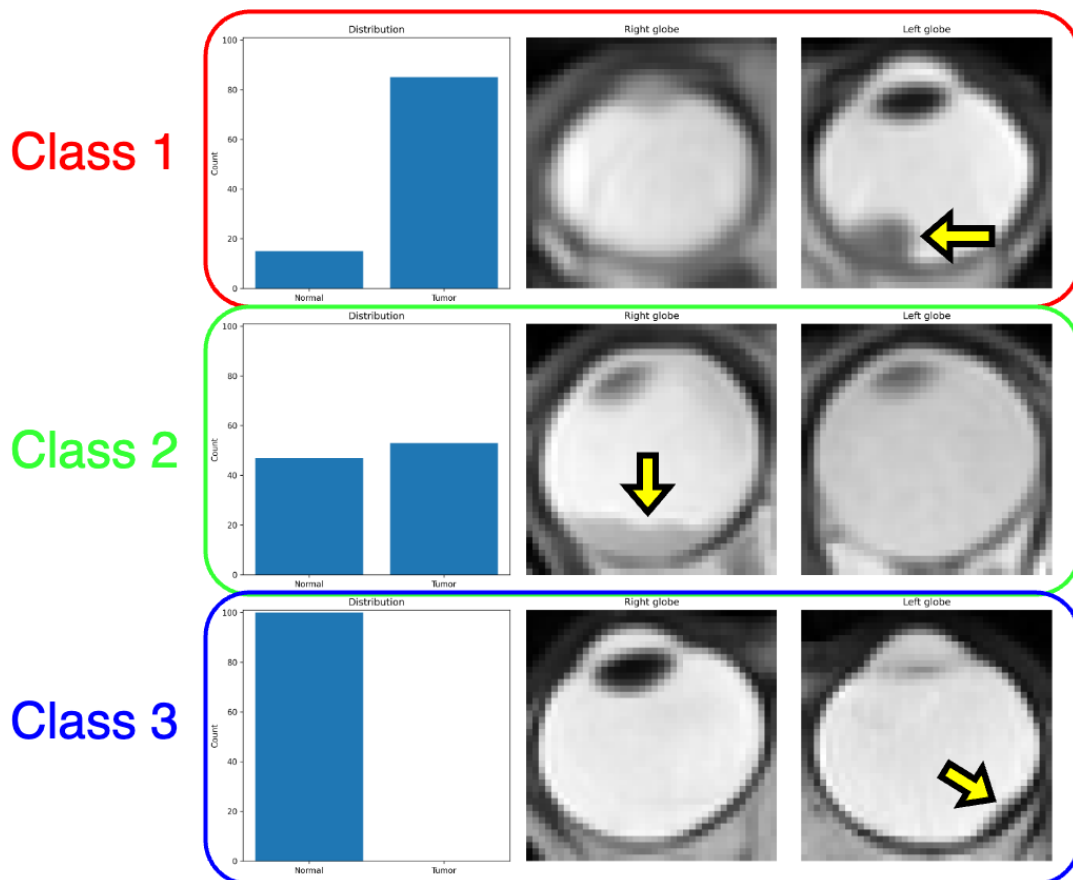


Figure 3: Examples of different uncertainties in tumor-containing cases. The top row displays an example from class 1, in which there is a correct prediction with low uncertainty (defined as being less than 20 %). Class 2, in the middle row, depicts a high-uncertainty scenario. We can see that the tumor is volume-averaged with the adjacent high T2 signal aqueous humor. As such the lesion is less contrastive within the image. Class 3, with an incorrect prediction of normal with low uncertainty, shows a small plaque-like lesion in the left globe that could easily be overlooked by a radiologist.

DropWeak Technique: An Empirical Study with Baresnet. *Diagnostics*, 13(4): 800.

Faghani, S.; Khosravi, B.; Zhang, K.; Moassefi, M.; Jagtap, J. M.; Nugen, F.; Vahdati, S.; Kuanar, S. P.; Rassoulinejad-Mousavi, S. M.; Singh, Y.; et al. 2022. Mitigating bias in radiology machine learning: 3. Performance metrics. *Radiology: Artificial Intelligence*, 4(5): e220061.

Faghani, S.; Moassefi, M.; Rouzrokh, P.; Khosravi, B.; Bafour, F. I.; Ringler, M. D.; and Erickson, B. J. 2023. Quantifying Uncertainty in Deep Learning of Radiologic Images. *Radiology*, 308(2): e222217.

Ferianc, M.; Maji, P.; Mattina, M.; and Rodrigues, M. 2021. On the effects of quantisation on model uncertainty in bayesian neural networks. In *Uncertainty in Artificial Intelligence*, 929–938. PMLR.

Gal, Y.; and Ghahramani, Z. 2016. Dropout as a bayesian approximation: Representing model uncertainty in deep learning. In *international conference on machine learning*, 1050–1059. PMLR.

Kendall, A.; and Gal, Y. 2017. What uncertainties do we

need in bayesian deep learning for computer vision? *Advances in neural information processing systems*, 30.

Ketkar, N.; Moolayil, J.; Ketkar, N.; and Moolayil, J. 2021. Automatic differentiation in deep learning. *Deep Learning with Python: Learn Best Practices of Deep Learning Models with PyTorch*, 133–145.

Lakshminarayanan, B.; Pritzel, A.; and Blundell, C. 2017. Simple and scalable predictive uncertainty estimation using deep ensembles. *Advances in neural information processing systems*, 30.

Lambert, B.; Forbes, F.; Tucholka, A.; Doyle, S.; Dehaene, H.; and Dojat, M. 2022. Trustworthy clinical AI solutions: a unified review of uncertainty quantification in deep learning models for medical image analysis. *arXiv preprint arXiv:2210.03736*.

McCordle, B.; Zukotynski, K.; Doyle, T. E.; and Noseworthy, M. D. 2021. A radiology-focused review of predictive uncertainty for AI interpretability in computer-assisted segmentation. *Radiology: Artificial Intelligence*, 3(6): e210031.

Panicek, D. M.; and Hricak, H. 2016. How sure are you,

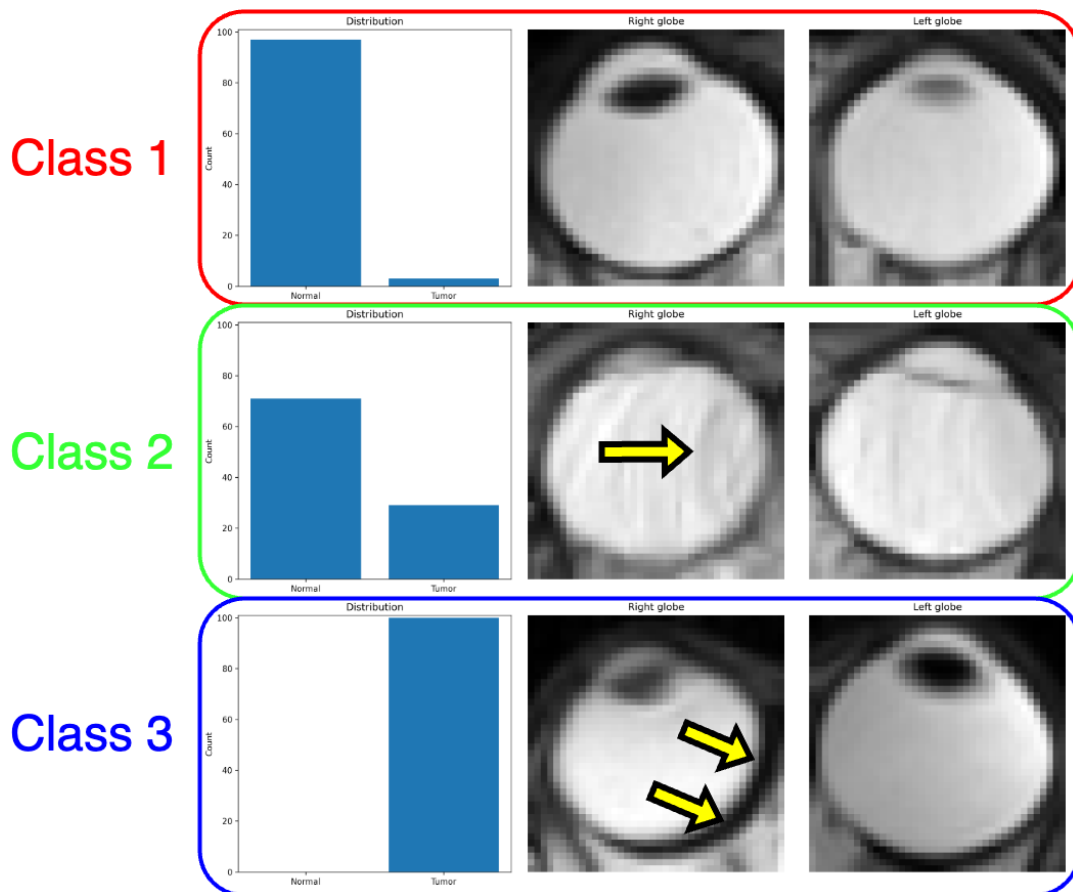


Figure 4: Examples of different uncertainties in normal, tumor-free cases. The top row displays an example from class 1, in which there is a correct prediction with low uncertainty (defined as being less than 20 %). Class 2, in the middle row, depicts a high-uncertainty scenario. We can see that that the motion and pulsation artifact creates a vague structure that could fool the algorithm into believing it may be a lesion. The class 3 example, which incorrectly predicts a tumor with low unlikelihood, displays apparent thickening at the posterior globe. Although this is due to volume averaging and slice selection, it can be seen to resemble a mass to the AI algorithm.

doctor? A standardized lexicon to describe the radiologist’s level of certainty. *American Journal of Roentgenology*, 207(1): 2–3.

Paszke, A.; Gross, S.; Massa, F.; Lerer, A.; Bradbury, J.; Chanan, G.; Killeen, T.; Lin, Z.; Gimelshein, N.; Antiga, L.; et al. 2019. Pytorch: An imperative style, high-performance deep learning library. *Advances in neural information processing systems*, 32.

Purkayastha, S.; Shalu, H.; Gutman, D.; Modak, S.; Basu, E.; Kushner, B.; Kramer, K.; Haque, S.; and Stember, J. 2022. Deep neuroevolution for limited, heterogeneous data: proof-of-concept application to Neuroblastoma brain metastasis using a small virtual pooled image collection. *arXiv preprint arXiv:2211.14499*.

Qendro, L.; Campbell, A.; Lio, P.; and Mascolo, C. 2021. Early exit ensembles for uncertainty quantification. In *Machine Learning for Health*, 181–195. PMLR.

Selvan, R.; Faye, F.; Middleton, J.; and Pai, A. 2020. Uncertainty quantification in medical image segmentation with

normalizing flows. In *Machine Learning in Medical Imaging: 11th International Workshop, MLMI 2020, Held in Conjunction with MICCAI 2020, Lima, Peru, October 4, 2020, Proceedings 11*, 80–90. Springer.

Spall, J. C. 1992. Multivariate stochastic approximation using a simultaneous perturbation gradient approximation. *IEEE transactions on automatic control*, 37(3): 332–341.

Stember, J.; Jenabi, M.; Pasquini, L.; Peck, K.; Holodny, A.; and Shalu, H. 2023. Deep neuroevolution to predict astrocytoma grade from functional brain networks. In *2023 5th International Conference on Intelligent Medicine and Image Processing (IMIP)*, 1–6. IEEE.

Stember, J. N.; and Shalu, H. 2022. Deep Neuroevolution Squeezes More out of Small Neural Networks and Small Training Sets: Sample Application to MRI Brain Sequence Classification. In *International Symposium on Intelligent Informatics*, 153–167. Springer.

Stember, J. N.; Young, R. J.; and Shalu, H. 2023. Direct Evaluation of Treatment Response in Brain Metastatic Dis-

ease with Deep Neuroevolution. *Journal of Digital Imaging*, 36(2): 536–546.

Stewart, R.; Nowlan, A.; Bacchus, P.; Ducasse, Q.; and Komendantskaya, E. 2021. Optimising hardware accelerated neural networks with quantisation and a knowledge distillation evolutionary algorithm. *Electronics*, 10(4): 396.

Such, F. P.; Madhavan, V.; Conti, E.; Lehman, J.; Stanley, K. O.; and Clune, J. 2017. Deep neuroevolution: Genetic algorithms are a competitive alternative for training deep neural networks for reinforcement learning. *arXiv preprint arXiv:1712.06567*.

Yang, S.; and Fevens, T. 2021. Uncertainty quantification and estimation in medical image classification. In *Artificial Neural Networks and Machine Learning–ICANN 2021: 30th International Conference on Artificial Neural Networks, Bratislava, Slovakia, September 14–17, 2021, Proceedings, Part III 30*, 671–683. Springer.

Zhou, B.; and Feng, J. 2018. Sample Efficient Deep Neuroevolution in Low Dimensional Latent Space.

Appendix A: Comparison to Monte Carlo Dropout

Within this supplementary segment, our exploration centers on contrasting Uncertainty Quantification (UQ) employing Deep Neuroevolution (DNE) with the methodology rooted in the Monte Carlo approach. The latter technique encompasses the utilization of a gradient-based optimizer for the training of CNNs, accompanied by the incorporation of dropout in both the training phase and the subsequent uncertainty estimation process. To start, we used essentially the same CNN architecture as for DNE, but we added a dropout layer for both branches after the first fully connected layers. We used a dropout probability of 0.5. We used stochastic gradient descent for optimization, with a learning rate of 0.001. Our objective function was the cross entropy loss. We trained the CNN for 5,000 epochs, after which convergence to 100% training set accuracy was achieved. As for DNE, we did two-fold cross-validation, with roughly even training:testing splits. Figure 5 shows the learning curve for one of the cross-validations. In particular, we note that the variance in testing set accuracy decreases from early during training to later when the system has converged. We can contrast this for DNE’s analogous curve (Figure 2), in which the variations in testing set accuracy also vary less than initially but with higher variance than for the Monte Carlo approach. This reduced variance is due to the overfitting that occurs during training with gradient-based methods and is reflected in Table 2. The table shows that, compared to DNE, Monte Carlo has a relative decrease in Class 2 (High uncertainty) even though there is a relatively large prediction error.

Appendix B: Single-branch CNN architecture

Part of our initial experimentation with various hyperparameter settings involved trying different network architectures. In particular, we initially studied the problem using a single-branch CNN, that took as input single orbital images (Figure 6). Ultimately, the branched architecture of Figure 1

UQ class	Tumor	Normal
Correct with low uncertainty	16 (48.4%)	9 (27.3%)
High uncertainty	6 (18.2%)	6 (18.2%)
Incorrect with low uncertainty	11 (33.3%)	18 (54.5%)

Table 2: Distribution of UQ classes. For purposes of evaluation, high uncertainty is formally defined here as Shannon entropy greater than 0.2.

performed better and we used the latter for UQ. We can rationalize this by the branched network’s added emphasis on symmetry between the orbits; in addition to extracting features of choroidal metastatic lesions, the dual branched scheme finds features that specifically reflect symmetry or breaking of symmetry. We studied cases in which only one orbit had metastatic disease. The choice reflects the fact that the vast majority of patients with choroidal metastatic disease have it in one eye only. Only one patient had bilateral choroidal metastases and this patient was thus excluded from our study. Given the unilaterality of choroidal metastases, symmetry breaking is an important hallmark of the condition.

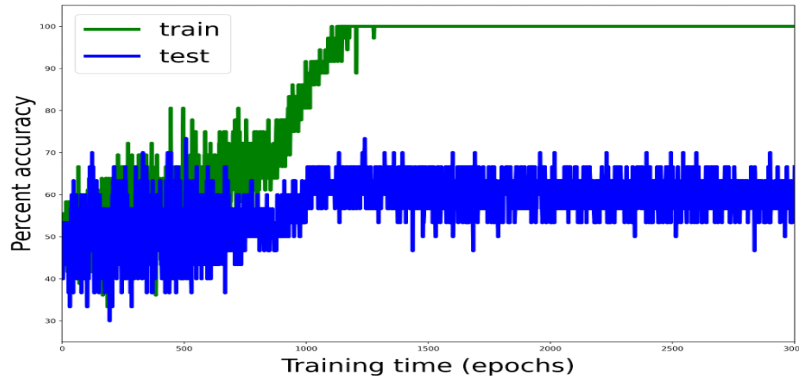


Figure 5: Learning curve during training of the CNN with gradient-based optimization and dropout (Monte Carlo approach).

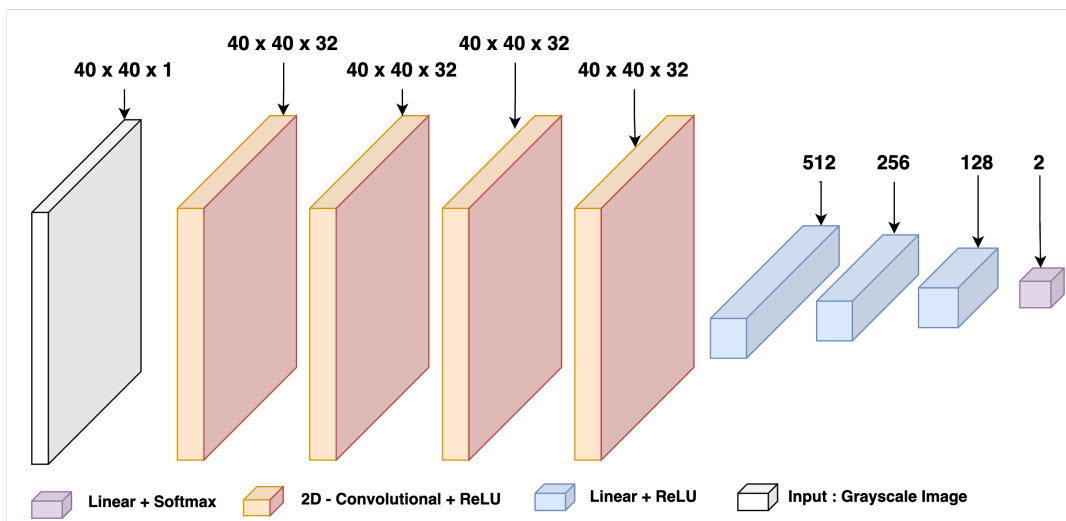


Figure 6: Single input neural network architecture used for the binary classification (tumor vs normal) of choroidal metastases from Brain MRI slices. The network takes as input a grayscale image of size $(40, 40, 1)$: (Height, Width, Channel) and produces a Softmax distribution over the respective classes of interest. Respective convolutional channels (for CNN layers) and Neuron counts (Linear layers) are marked against each block. Respective hyperparameters used in training the network as per Algorithm 1 : $\{\alpha = 0.12, p = 40, N_{epochs} = 10^5, R_{max}^{Dr} = 30 \text{ or } 36\}$